ACS Partner Journal

CHEMICAL & BIOMEDICAL IMAGING

pubs.acs.org/ChemBioImaging

Article

Developing Multichannel smFRET Approach to Dissecting Ribosomal Mechanisms

Published as part of Chemical & Biomedical Imaging virtual special issue "Sub-diffraction Chemical Imaging".

Ran Lin and Yuhong Wang*

Cite This: *Chem. Biomed. Imaging* 2024, 2, 501−509

Read Online

ACCESS | Metrics & More | Article Recommendations | Supporting Information

ABSTRACT: The ribosome, a 2.6 megadalton biomolecule measuring approximately 20 nm in diameter, coordinates numerous ligands, factors, and regulators to translate proteins with high fidelity and speed. Understanding its complex functions necessitates multiperspective observations. We developed a dual-FRET single-molecule Förste Resonance Energy Transfer method (dual-smFRET), allowing simultaneous observation and correlation of tRNA dynamics and Elongation Factor G (EF-G) conformations in the same complex, in a 10 s time window. By synchronizing laser shutters and motorized filter sets, two FRET signals are captured in consecutive 5 s intervals with a time gap of 50−100 ms. We observed distinct fluorescent emissions from single-, double-, and quadruple-labeled ribosome complexes. Through comprehensive spectrum analysis and correction, we distinguish and correlate conformational changes in two parts of the ribosome, offering additional perspectives on its coordination and timing during translocation. Our setup's versatility, accommodating up to six FRET pairs, suggests broader applications in studying large biomolecules and various biological systems.

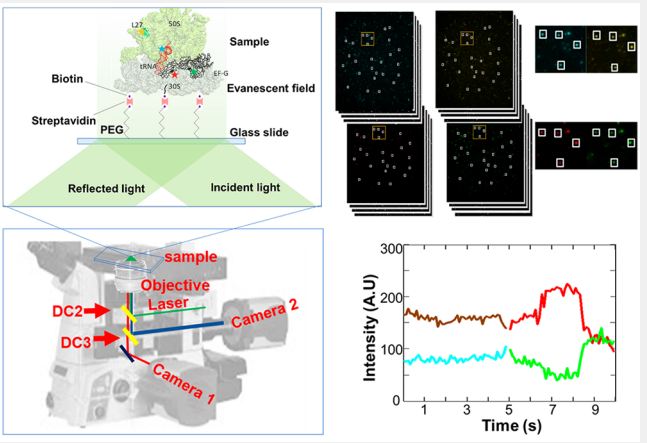

KEYWORDS: *Dual-smFRET, multichannel smFRET, ribosome translocation, spectrum crosstalk, TIRF microscope, allosteric interaction*

INTRODUCTION

Förster Resonance Energy Transfer (FRET) is a process where energy transfers between two fluorophores, named the donor and the acceptor. The ideal separation distance for this interaction is between 2 to 8 nm, with the transfer efficiency being inversely proportional to the sixth power of their separation distance.[1] This efficiency is conveniently quantifiable through the fluorescence intensity measurement and is highly sensitive to distance changes. Consequently, FRET has become an indispensable tool for studying the dynamics and conformational changes of biomolecules, where nanometer-scale distance variations are essential for biofunctions. Due to its ability to measure changes in distances between paired dyes attached to different or different parts of biomolecules, FRET is also referred to as an "optical ruler".[2]

To uncover the often-inhomogeneous subpopulations within biomolecules, FRET is integrated with single-molecule techniques.[3] This combination effectively eliminates the effects of ensemble averaging, thereby significantly enhancing our understanding of biomolecules at the individual level. One pioneering example in the ribosome field is the identification of multiple hybrid states via tRNA-to-tRNA FRET pairs.[4,5] The ribosome is the universal protein synthesis device in all three domains of life forms.[6] In bacteria, it is composed of a large and a small subunit, named 50S and 30S, respectively (Figure 1). Each subunit comprises RNA−protein assemblies, with the total molecular weight being approximately 2.6 MDa. The distance between the entry and exit sites of tRNA on the ribosome exceeds 26 nm, which is significantly greater than the detection range of a single FRET pair. Protein synthesis proceeds in four stages: initiation, elongation cycle, termination, and recycling. Each stage involves global and local ribosomal dynamics while it interacts with various ligands, factors, and regulators.[7−13] Some of the factors are shown in Figure 1, such as IF1, 2, 3; EF-Tu; EF-G; RF1/2, 3; and RRF. Eukaryotic ribosomes are more complex, involving a greater number of these factors. Multiple-perspective FRET pairs have

Received: January 29, 2024
Revised: March 10, 2024
Accepted: March 11, 2024
Published: March 21, 2024

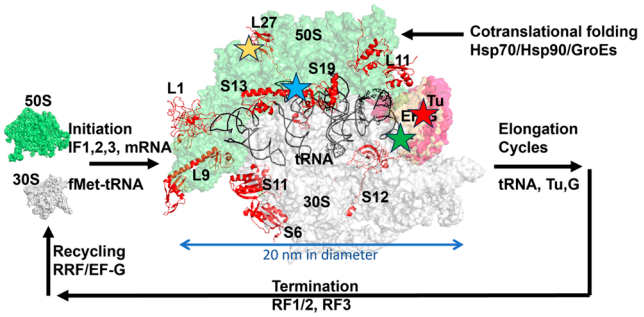

Figure 1. Four stages of ribosomal protein synthesis: initiation, elongation cycles, termination, and recycling. Some proteins used for smFRET studies are shown in the ribbon model. "S#" are proteins on the small subunit (S13), and "L#" are proteins on the large subunit. tRNAs at A-, P-, and E-sites are depicted in black-colored wireframe models. EF-Tu (yellow) is depicted in the accommodation stage with a tRNA at the A/T site. The Tu binding site overlaps with that of EF-G, which is depicted as magenta. The ribosome 50S, 30S, EF-Tu, and EF-G are depicted as surface. The structures are aligned from 4v67, 4v5g, and 7pjv. The size of the ribosome is about 20 nm in diameter. The stars depict the FRET labelings used in this study.

been employed to study the cooperative dynamics underlying ribosomal functions, such as between S12−S19, S11−S13, S6-L9, S13−L1, S13−L5.[14−16] Additional ribosome dynamics are obtained by tracking the active ligands like tRNAs as they constantly move through the channel formed between the large and small subunits.[17−19] However, a caveat in these studies is that each of these FRET pairs is introduced and observed in isolation. As a result, the correlations of the experimental data among different FRET pairs do not come from the same ribosomal complexes. This can introduce challenges and variations to integrate these data to form a comprehensive depiction of the ribosomal function. Key aspects of concurrent and cooperative interactions occurring at various parts of the ribosome may not be fully captured by examining individual FRET pairs in isolation. A pioneering four-color smFRET experiment investigated the dynamics of DNA Holliday junctions. However, multi-FRET pair usage remains uncommon compared to two-color FRET, with no studies yet resolving multiple FRET pairs within the same ribosome or other large biomolecules.[20−22]

To address this limitation, we developed and characterized a dual-smFRET method to correlate the tRNA and EF-G conformations in the same ribosome complex. This method will be useful to provide coordination and timing of ribosomal dynamics allosterically, complementary to the current methods. Furthermore, it would allow tracking of multiple FRET pairs within the same biological systems beyond ribosome, such as DNA polymerase, nonribosomal peptide synthetases, chromosomes, etc.

RESULTS AND DISCUSSION

Dual smFRET TIRF System

In this setup, two distinct laser lines, operating at 532 and 488 nm, are used (Figure 2A). Each laser beam is guided through a dedicated pair of steering mirrors to facilitate alignment. Following these mirrors, the polarization of each laser beam is adjusted using a combination of a quarter-wave plate and a polarizer. These two beams are subsequently merged into a collinear path by a dichroic mirror (DC1). The combined beam is then passed through a beam expander with a spatial filter (50 nm pinhole) to both enlarge and refine the laser spot. Then the laser beam is directed through a long-focal distance lens, which focuses it into the back focal plane of the TRIF objective, after being reflected by a second dichroic mirror (DC2). The focused laser within the objective's back focal plane can be precisely manipulated via a mirror mounted on a motorized 2D translational stage, allowing fine-tune of the total internal reflection angle. This total reflected laser beam generates an evanescent wave that excites the samples above the objective in a thin region close to the glass coverslip's surface (~100 nm). The emitted fluorescence from the sample is then collected back through the same objective lens. The emission light passes through DC2, then splits at DC3. The acceptor fluorescence emission passes through DC3 and is directed to camera 1, while the donor fluorescence emission is reflected at DC3 and channeled to camera 2. Specific filters are installed within filter cubes to enhance the quality of the captured fluorescence signals. These filter cubes are mounted

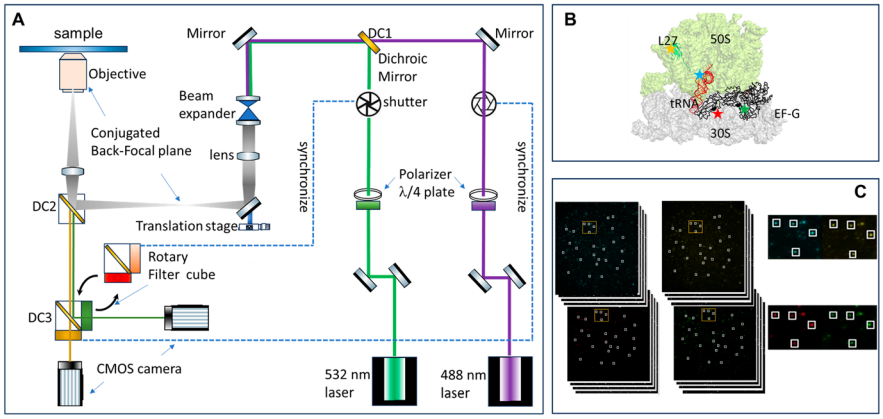

Figure 2. Dual FRET setup, sample, and images. (A) Schematic illustration of the two-laser multichannel TIRF microscope. (B) Illustration of the Cy3−Cy5 labeled ribosome in complex with Alexa488/594 labeled EF-G. The color and labeling positions of the dyes are Cy3-L27-yellow; Cy5-tRNA-Cyan; Alexa488/594-EF-G-green/red. (C) Time-lapsed movie series capturing the fluorescence emissions from the two FRET pairs. The left and right movies are combined, and the top and bottom movies are concatenated chronologically. A closeup view of the identified emissions are shown, where the emission of the different pairs are aligned perfectly from stage 1 and stage 2 aquisition and registered the same from the acceptor channel to the donor channel. Fitted traces are shown in Figure 5.

https://doi.org/10.1021/cbmi.4c00010
Chem. Biomed. Imaging 2024, 2, 501−509

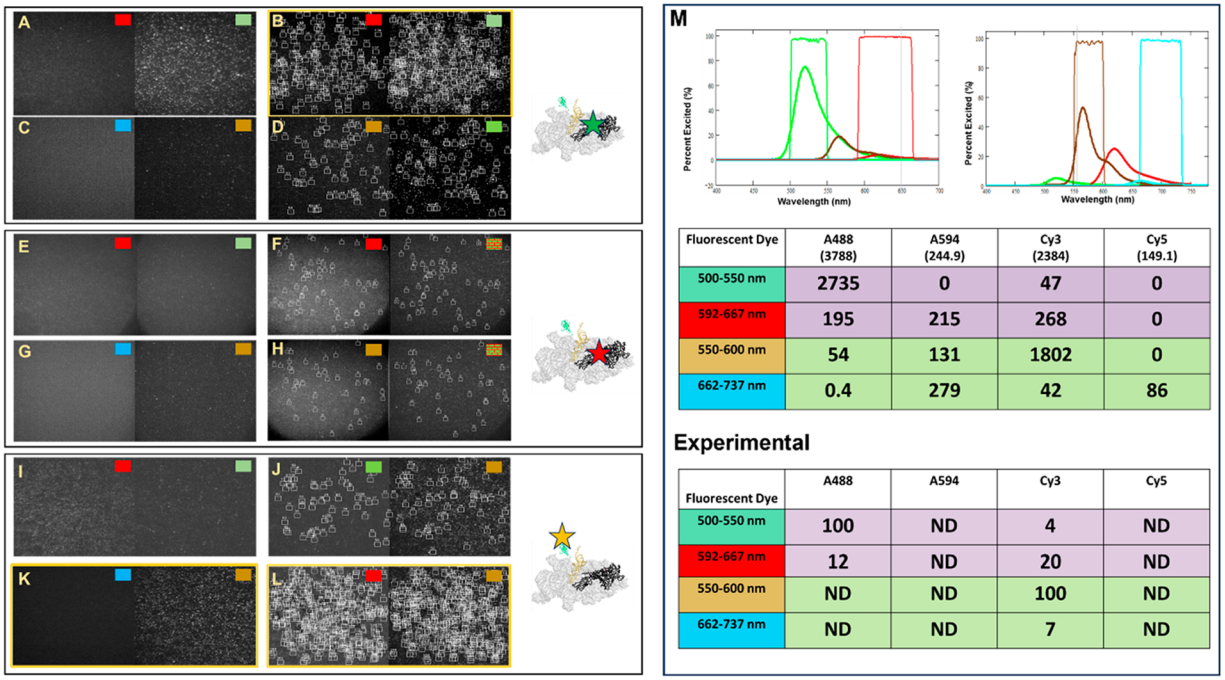

Fluorescent Dye	A488 (3788)	A594 (244.9)	Cy3 (2384)	Cy5 (149.1)
500-550 nm	2735	0	47	0
592-667 nm	195	215	268	0
550-600 nm	54	131	1802	0
662-737 nm	0.4	279	42	86

Experimental

Fluorescent Dye	A488	A594	Cy3	Cy5
500-550 nm	100	ND	4	ND
592-667 nm	12	ND	20	ND
550-600 nm	ND	ND	100	ND
662-737 nm	ND	ND	7	ND

Figure 3. Spectrum crosstalk in singly labeled ribosome complexes. The solid-colored small blocks label the receiving channels under Set1 or Set2 conditions, with the same color codes as in (M). The patterned blocks in (F) and (H) label the red receiving channel under 532 nm laser illumination. (A, C) representative image for Alexa 488 labeled EF-G under Set2 and Set1 conditions, respectively. (B) FRET pair identification of image A. The numbered boxes depict the paired emissions from the acceptor and donor channel. (D) FRET pair identification of recombined images of channels Cy3 and Alexa 488. (E, G) Representative images for Alexa 594 labeled EF-G under Set2 and Set1 conditions, respectively. (F) FRET pair identification of recombined images of channels Alexa 594 (Set2 condition) to Alexa 594 under 532 nm illumination. (H) FRET pair identification of recombined images of channels Cy3 (Set1 condition) to Alexa 594 under 532 nm illumination. (I, K) Representative image for Cy3 labeled L27 under Set2 and Set1 conditions, respectively. (J) FRET pair identification of recombined images of channels Alexa 488 and Cy3. (L) FRET pair identification of recombined images of channels Alexa 594 and Cy3. (M) Theoretical and experimental dyes' crosstalks, including theoretical emission spectra and filter windows.

on a motorized turret, and the position of the filter cubes are synchronized with the laser shutter, controlled by the camera TTL signal. Therefore, under 532 nm illumination, the cameras receive Cy5/Cy3 fluorescence emission in camera 1 and 2, respectively (Set1, 20 mW, filters "662−737 nm" and "550−600 nm"), and under 488 nm illumination, the cameras receive Alexa488/Alexa594 fluorescence emission in camera 1 and 2 (Set2, 20 mW, filters "592−667 nm" and "500−550 nm"), respectively. The images collected in camera 1 overlap perfectly across the two filter settings. But images collected in camera 2 display a mis-overlapping because of the minor positional shift of the DC3 component in the two different cubes, or the suboptimal positioning of the motorized turret, which houses the filter cubes. The details to correct this mismatching are outlined below.

We assembled a ribosome initiation complex for dual-FRET analysis. The tRNA P-site is occupied by a Cy5-labeled formylmethionyl-tRNA (Cy5-fmet-tRNA^{fMet}), and the ribosomal protein L27 is tagged with Cy3 dye. This FRET pair monitors the position of the P-site tRNA. Additionally, Alexa 488/594 double-labeled EF-G at the F411C/Y535C positions is introduced to the ribosome, resulting in a dual-FRET labeled ribosome complex. This complex is immobilized onto a coverslip glass surface that had been previously passivated with streptavidin. The immobilization is mediated via the 5′-biotinylated mRNA in the ribosome binding to the streptavidin on the surface (Figure 2B). Data collection occurred in two stages. In the first stage, 50 frames of images are collected at 100 ms exposure time with both cameras, using configuration Set1. During the second stage, an additional 50 frames are captured with both cameras under configuration Set2. Following data collection, the two data sets are first processed separately, then combined into one movie series. In each data set, the images from both cameras are cropped to an offset of "0" for both X- and Y-positioning, ensuring precise alignment of the emissions from the FRET pair. Subsequently, the two cropped sequences are horizontally combined to form a composite movie series with two channels (acceptor/donor). These movie series from the two sets are then concatenated chronologically, resulting in a final compounded movie series of 100 frames (100 ms/frame) with two channels side-by-side (Figure 2C). The first 50 frames represent data set1, and the following 50 frames are from data set2. The prealigning step prior to the concatenation addresses the earlier mentioned issue of positional shift of the DC3 component in the filter setup.

Figure 2C shows the image reconstruction. The top two time series are Cy5 and Cy3 emission images, respectively; the bottom two are Alexa594 and 488 emission images. The final movie consists of 100 frames and two channels. The closeup image in Figure 3C depicts the identified FRET pairs in the first and second set of 50 frames for Cy5/Cy3 and Alexa 488/594 pairs, respectively. Representative fitted traces of time-lapsed fluorescence intensities are shown in Figure 5. Thus, two FRET pairs on the same ribosome complex are fitted within the same time-lapse trace for a direct correlation

https://doi.org/10.1021/cbmi.4c00010
Chem. Biomed. Imaging 2024, 2, 501−509

Table 1. Counts of Emission Spots and FRET Pairs[a]

dye	Counts in channel		FRET pair /(percentage)	Figure label
Alexa 488	508	2437	220/(9%)	3B
	409	2437	96/(4%)	3D
Alexa 594	542	1076	59/(5%)	3F
	595	1076	41/4%	3H
Cy3	656	2749	190/(7%)	3J
	1700	2749	878/(32%)	3L

[a]FRET pairs are color coded the same as in Figure 3. The FRET pairs are due to spectrum leakage from the ribosome complexes.

analysis. The switching time between the rotary filter cube is 50−100 ms, enabling 200 ms-resolved images every other 100 ms in Set1 and 2 alternatively. This resolution is suitable for observing a wide range of biological processes. However, our study chose to focus on a static ribosome initiation complex to simplify the demonstration of our method. In a dynamic setting, a single sample channel supports only one movie, whereas in a static setting, it accommodates hundreds of movies from different fields. This is also critical with regard to the limited ribosome materials. By using a static complex, we aim to clearly present the fundamental feasibility of this method, paving the way for future dynamic experiments.

Experimental Measurement of Crosstalk

Quantifying spectral crosstalk among the four dyes (Cy3, Cy5, Alexa488, and Alexa594) is more complex compared to single FRET-pair experiments because of the unintentional excitation of the additional FRET pair, which can generate signals in the current channels. To address this issue, we measured complexes individually labeled with each of the four dyes. Notably, Cy5 produced no detectable signal in either data acquisition stage and is thus excluded. The emission spectra for the remaining three dyes are shown in Figure 3 (enlarged images are shown in Supporting Information).

Each block describes a singly labeled ribosome complex with four combined images displayed. The left two images are obtained using the dual FRET configuration previously described: the top set with Set2 (blue laser + Alexa 594/488 filter set) and the bottom set with Set1 (red laser + Cy5/Cy3 filter set). The images are arranged as acceptor/donor from left/right, respectively. The two right images fit FRET pairs of differently recombined channels to assess potential crosstalk, with the singly labeled dye images positioned on the right as donors. Images in Figure 3B, D, F, H, J, and L are labeled with small blocks for easy reference to specific filter channel results. Table 1 summarizes emission spots and FRET-pairs. For example, Figure 3B has 2437 Alexa 488 spots with 220 pairing in the Alexa 594 channel, totaling 508 spots there. This indicates approximately 9% leakage of the Alexa 488 into the 549 channel. Conversely, only ∼4% (96/2437) leakage into the Cy3 channel is observed, deemed negligible, as it is below the 5% threshold (Figure 3D). Figure 3E and G reports minimum signals for Alexa 594 across channels under Set1 and 2 conditions. With 1076 ribosome molecules identified in the 594 channel under 532 nm illumination, these observations suggest negligible leakage of Alexa 594 dye in any channels. Lastly, Cy3 dye leaking into all three other channels is observed (Figure 3J, L).

Leakage percentages are calculated as "$I_{acceptor}/I_{donor}$", using the fitted intensities from the left and right panels of the combined images. The histograms of the leakage analysis are depicted in Figure 4. Figure 4A−D show leakages from Figures 3B, D, J, and L. Negligible leakage is observed in Figure 4B, presenting a flat histogram. Fitted leakage values are detailed in Figure 3M and incorporated in FRET efficiency calculations. (In all FRET efficiency histograms, the dotted lines represent the Gaussian-fitting curves.)

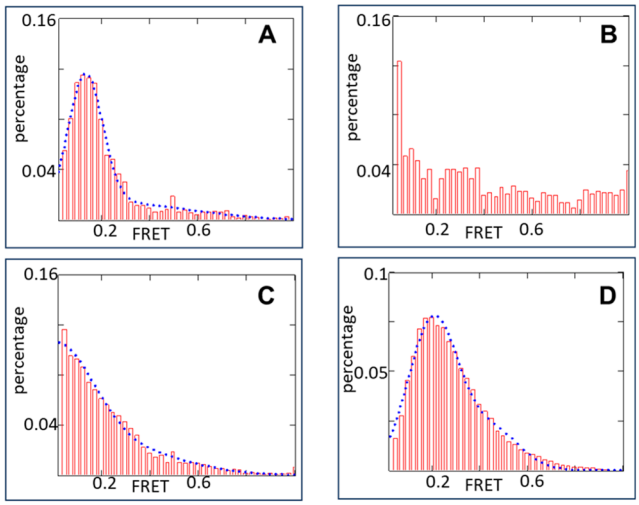

Figure 4. Crosstalk quantification of singly labeled ribosome complexes. (A) Crosstalk of Alexa 488 to channel Alexa 594. (B) Crosstalk of Alexa 488 to channel Cy3. (C) Crosstalk of Cy3 to channel Alexa 488. (D) Crosstalk of Cy3 to channel Alexa 594.

Theoretical Estimation of Crosstalk

Figure 3M also illustrates the theoretical emission spectra of the dyes under 488 nm (left) and 532 nm (right) laser illumination. These spectra are adjusted for excitation and emission efficiencies using corrected data from the SpectraViewer tool by ThermoFisher, filter transmission percentages using Chroma product spectra, and camera quantum yields within the filter ranges using Hamamatsu technical notes (Supporting Information). However, they do not account for experimental variables like laser power, or dye environment in the biomolecule, etc. Despite this, they serve as useful references for comparing experimental data. Theoretical emission intensities within the filter windows are totaled and presented beneath the plots, after being corrected with the filter transmission percentage and camera quantum yield. The

https://doi.org/10.1021/cbmi.4c00010
Chem. Biomed. Imaging 2024, 2, 501−509

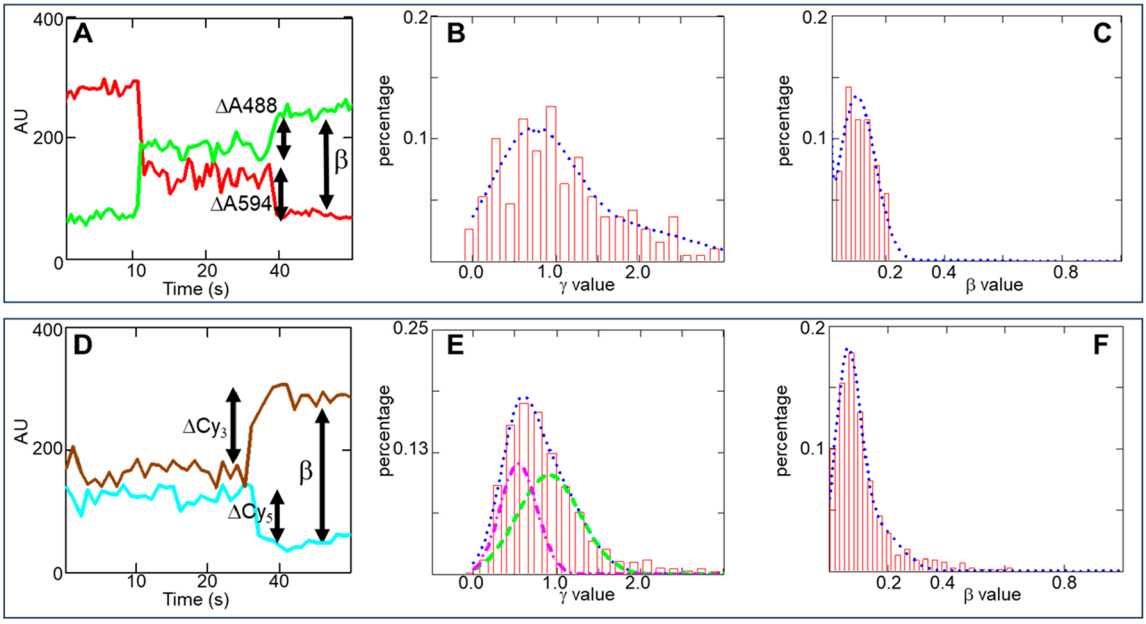

Figure 5. Measurement of γ and β. (A, D) Representative traces to measure gamma and beta values in Alexa 488/594 and Cy3/Cy5 FRET pairs, respectively. (B, E) Histograms of gamma values in Alexa 488/594 and Cy3/Cy5 FRET pairs, respectively. (C, F) Histograms of beta values in Alexa 488/594 and Cy3/Cy5 FRET pairs, respectively. The dotted lines are fittings with Gaussian functions.

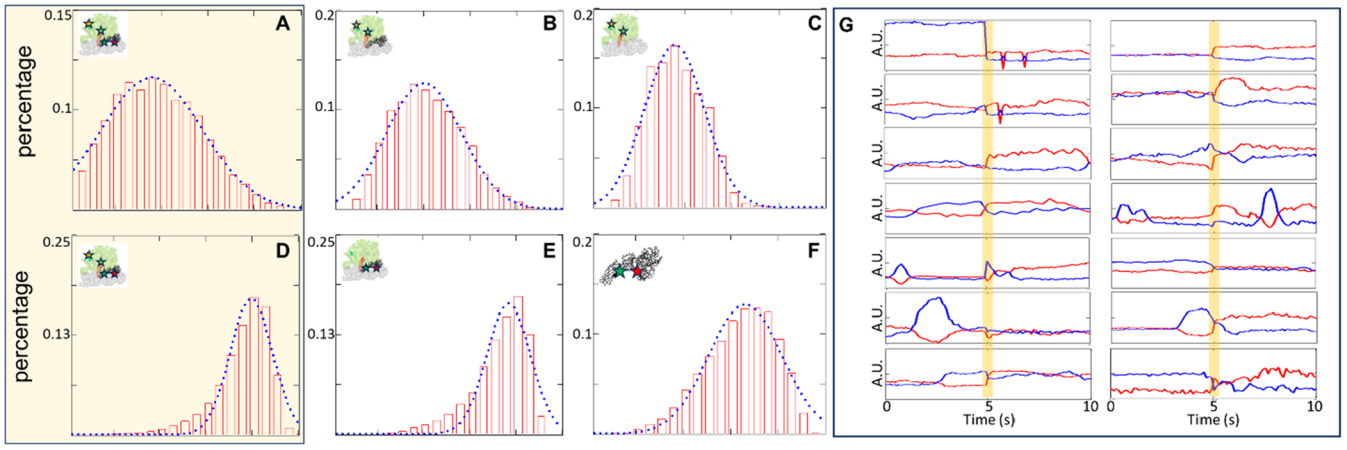

Figure 6. Dual and single FRET measurement of ribosome complexes. (A, D) FRET efficiency histogram of the Cy3−Cy5 FRET pair between fMet-tRNA and L27, and Alexa 488−594 FRET pair in the double labeled EF-G, respectively. Both FRET pairs are observed in the same ribosome complex and the same time-lapse trace. (B) FRET efficiency histogram of the Cy3−Cy5 FRET pair between fMet-tRNA and L27. The ribosome complex is bounded with unlabeled EF-G. (C) FRET efficiency histogram of Cy3−Cy5 FRET pair between fMet-tRNA and L27. The ribosome complex is not bounded with unlabeled EF-G. (E) FRET efficiency histogram of Alexa 488−594 FRET pair in double-labeled EF-G. The ribosome complex is charged with unlabeled fMet-tRNA and L27. (F) Free double labeled EF-G. The tethering is via 6xHis-tag specific biotinylated antiobody. (G) Representative traces of fluorescence emissions fitted from dual FRET labeled ribosome complex that generate histograms of A and D. The red and blue traces are for acceptor and donor, respectively. The first 5 s are traces from the Cy3−Cy5 FRET pair, and the second 5 s are traces from the Alexa 488−594 FRET pair.

first two rows show the emission compositions under Set1 configuration, while the third and fourth rows correspond to Set2 configuration. From a theoretical perspective, the leakage from dye Alexa 488 to the Alexa 594 channel is around 195/2735 (7%, with an experimental value of 12%). The leakage of Cy3 to the Cy5 channel is about 42/1802 (2%, experimental 7%). Its leakage into the Alexa 594 and 488 channels is 15% and 3%, respectively, compared to experimental values of 20% and 4%, respectively. While there are discrepancies between the experimental and theoretical values, they show a maximum of 2-fold differences. These experimental data are utilized in the fluorescence intensity correction in Figure 6.

γ and β Measurement

The γ parameter corrects for differing detection sensitivity in the acceptor/donor channel, and β corrects for donor spectrum crosstalk into the acceptor channel.[23] The final FRET value is calculated by

$$\mathrm{FRET} = \frac{I_A - I_D \times \beta}{I_A - I_D \times \beta + I_D \times \gamma} \quad (1)$$

https://doi.org/10.1021/cbmi.4c00010
Chem. Biomed. Imaging 2024, 2, 501−509

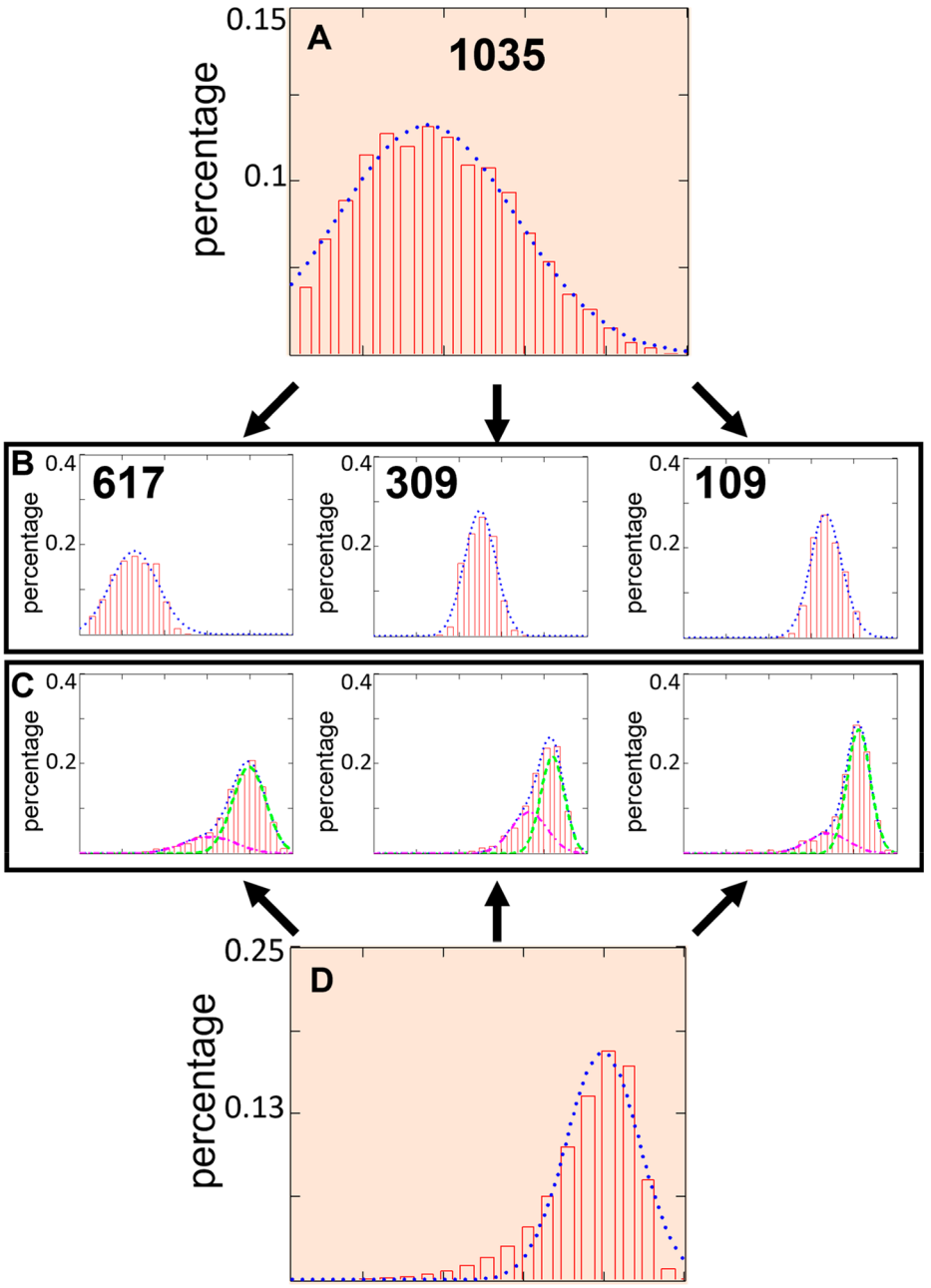

Figure 7. Subpopulation sorting and correlation analysis. (A) The tRNA-L27 FRET efficiency histogram for 1035 ribosomes. (B) Sorting of ribosome particles based on the positions of tRNA relative to L27. (C) Correlated EF-G subpopulations extracted from the second 5 s data, embedded in ribosome subpopulations from (B). (D) The overall histogram of the EF-G molecule prior to sorting.

In this equation, the I_A and I_D are adjusted by using the crosstalk corrections previously discussed. The γ and β values are derived from traces in Figure 5A and D, after acceptor photobleaching.[23] γ is calculated from the ratio of δA (before and after the bleaching) to δD (after and before the bleaching), and β is calculated from the ratio of (I_A) to (I_D) after bleaching. Measured γ values for the Alexa 488/594 and Cy3/Cy5 FRET pairs are 0.75 and 0.78, respectively (Figure 5B and E); corresponding β values are 0.12 and 0.07, respectively (Figure 5C and F). These values are plugged into eq 1 to calculate the final FRET efficiencies in Figure 6.

Dual FRET Measurement

For method development, we chose the simplest static ribosome complex with only the initiation tRNA at the P-site. A functionally impaired EF-G mutant is trapped on this ribosome with fusidic acid.[24−27] Figures 2B and 6A and D depict the arrangement of these dual-FRET pairs.

Figure 6A shows a FRET efficiency histogram for the Cy5−fMet-tRNA and Cy3−L27 pair, featuring 1035 particles with a broad Gaussian distribution centered at 0.4 ± 0.2. With a Förster distance of 6 nm for both FRET pairs (as per ThermoFisher and ref 28), this FRET value implies a distance of 6.4 nm, which is 1.3 nm longer than the distance estimated from crystal structure 4v67.[29] Previously, we have reported a

https://doi.org/10.1021/cbmi.4c00010
Chem. Biomed. Imaging 2024, 2, 501−509

FRET value of 0.63 for the P-site Cy3-tRNA and Cy5-L27 pair, consistent with structural prediction.[19] This discrepancy may arise from several factors: 1. Different dye linkers from various vendors may affect the Förster distance; 2. Swapped dye labeling positions compared to our previous studies, which is known to affect FRET values;[30] 3. Filter window settings affect the signal intensities; and 4. Use of different cameras. Because of these variances, the FRET value is within the expected experimental variations. The broad distribution can be due to noise, inherent in single molecule data, or more significantly, to the dynamics between the tRNA and L27, as the ribosome exhibits high flexibility influenced by EF-G.[27] This distribution, potentially indicating more than one biological species, can be fitted with multiple peaks, as we observed before.[19] Further analysis is given in Figure 7. Unlike the tRNA-L27 pair's broad distribution, the double-labeled EF-G in the same complexes shows a narrower distribution centered at 0.8 ± 0.1 (Figure 6D), implying a distance of 4.7 nm, about 1 nm longer than indicated by 7pjv. Histograms in Figure 6A and D are derived from traces like in Figure 6G, where the first and second 5 s data segments correspond to the Cy3/Cy5 and Alexa 488/594 FRET pairs, respectively.

Figure 6B (1663 particles) and 6E (865 particles) demonstrate that dual FRET pairs in the same complex do not affect each other's signal. In Figure 6B, only the Cy3−Cy5 FRET pair is present, with EF unlabeled. In Figure 6E, only the Alexa 488/594 FRET pair is present with the ribosome unlabeled. These single-FRET experiments yield FRET efficiency histograms nearly identical to those in Figure 6A and D, in terms of both center and sigma values. Additionally, Figure 6C (865 particles) demonstrates the FRET histogram of a labeled ribosome initiation complex only. In comparison to Figure 6A and B, the Gaussian distribution in Figure 6C has the same average FRET value of 0.4, but with half the sigma, suggesting less signal fluctuation. This result serves as a control, consistent with the proposed reason for the Gaussian broadening in Figure 6A. It is generally accepted that EF-G stabilizes the ribosome in the ratchet state, where the small subunit rotated counterclockwise relative to the large subunit.[20] This rotation and other movements allow for greater conformational flexibility, facilitating mRNA−tRNA movement during translocation. Therefore, it is reasonable that the binding of EF-G allows more dynamic motion of the initiation tRNA at the P-site, leading to a broader dispersion observed in Figure 6A and B.

Figure 6F (1168 particles), featuring only EF-G without the ribosome, shows a FRET efficiency histogram with the center shifted from 0.8 to 0.7 and an increased sigma from 0.1 to 0.2. These shifts suggest that free EF-G, not bound to any nucleotide, is flexible, in contrast to EF-G bound on the ribosomes in Figure 6D and E.

Sorting Subpopulations with Dual FRET Data

When both FRET pairs originate from the same complex, additional information can be obtained. Subpopulations can be first sorted based on one FRET pair, enabling correlation analysis with the other pair. For example, this can reveal how the EF-G conformational changes affect tRNA configurations. Such analysis is valuable for understanding sequential events, as demonstrated in Figure 7. The tRNAs inside the cleft between the large and small ribosomal subunits take many intermediate states during translocation. Time-resolved Cryo-EM studies have identified 50 distinct tRNA intermediate states, and X-ray structures provided detailed transitions of tRNA.[31−33] Therefore, we sort the subpopulations based on the Cy3-Cy5 FRET pair, which reports the tRNA intermediate positions. Smaller FRET values suggest fMet-tRNA at A/P state further from P-site, and larger values indicate a closer distance to the P-site, as L27 is closer to P-site tRNA. The 1035 traces depicted in Figure 6G comprise two data sets: the first 50 points represent fluorescence intensities for the Cy3-Cy5 pair, and the second 50 points correspond to fluorescence intensities for the Alexa 488−594 pair. The FRET efficiencies are obtained according to eq 1. After that, the FRET efficiency traces are sorted as the following: initially, the first 50 FRET efficiency values are averaged and categorized into three distinct ranges (0−0.3, 0.3−0.6, 0.6−1.0), creating three subpopulations. Subsequently, for each subpopulation, the first and second sets of 50 FRET efficiency points are analyzed to generate histograms. Sorting identified 617, 309, and 109 ribosomes with Cy3−Cy5 FRET efficiency histograms centered at 0.26, 0.50, and 0.67, respectively, indicating three grouped tRNA binding sites (Figure 7B). Then EF-G conformations in these subpopulations are extracted from the second half of the time-lapse traces (Figure 7C). The fitting parameters for the EF-G's FRET efficiency histograms are in Table 2, revealing two FRET states: 0.65 and 0.8. There are slight but discernible EF-G changes in the different subpopulations. The EF-G conformational changes coupled to ribosome translocation are intensively studied, but the precise mechanisms remain debated.[6,8,14,20,24,34−37] Sorting and correlating between tRNA positions and EF-G conformations, as depicted in Figure 7, shed light on the mechanism. As summarized in Table 2, the proximity of tRNA to the ribosomal protein L27 at the central protuberance, indicated by increased FRET efficiencies between Cy3−Cy5 dyes, correlates with EF-G adopting a more compact conformation and reduced flexibility, as evidenced by a higher percentage of high FRET species and a narrower Gaussian distribution. These findings, though derived from an initiation complex that cannot translocate, can be extrapolated to normal pretranslocation complexes, suggesting a mechanism by which EF-G facilitates translocation. Additional biological insights from this method have been reported recently, offering further understanding of the intricate dynamics involved in ribosome function.[38]

Table 2. Fitting Parameters for smFRET Alexa 488−594 in Figure 7C

Subpopulation numbers		617	309	109
Cy3-Cy5 FRET value		0.26	0.50	0.67
FRET value 0.65	percentage	18%	17%	12%
	sigma	0.14	0.07	0.09
FRET value 0.8	percentage	82%	83%	88%
	sigma	0.08	0.07	0.06

CONCLUSION

In this study, we developed and characterized a dual-smFRET methodology to correlate the tRNA and EF-G conformations in the same ribosome complex. We have established essential optical setup details as well as comprehensive spectrum crosstalk analysis and correction methods. We present example dual-FRET data, demonstrating the capability to sort and correlate conformational changes between tRNA-L27 and EF-

https://doi.org/10.1021/cbmi.4c00010
Chem. Biomed. Imaging 2024, 2, 501−509

G. This method has the potential to elucidate the coordination and timing of ribosomal dynamics, contributing to a deeper understanding of translational fidelity and efficiency. Its applicability can be extended to screening antibiotics or studying resistance mechanisms, as many antibiotics target tRNA binding sites or EF-G. Additionally, the rotary turret is designed to hold 6 filter cubes, enabling the potential introduction of 6 FRET pairs to a single ribosome complex, with each cube collecting data from one pair. Above this turret, a second turret, depicted in the table of contents graph, can host 6 distinct laser reflecting cubes for various laser illuminations. Synchronizing both turrets and laser shutters allows the camera to collect data from all 6 FRET pairs alternatively. With careful spectrum correction, as demonstrated herein, more FRET pairs can be introduced to large biomolecules, extending beyond ribosomes, although spectrally resolving 6 FRET pairs can be challenging in practice. Furthermore, this method allows for tracking of different FRET pairs at allosteric positions in real time, simultaneously or with minimal time gaps, through feasible modifications. This capability opens new avenues for studying various protein-to-protein interactions, enzyme activities, and other cellular processes across multiple locations concurrently.

METHODS

Materials

The inverted microscope is a Nikon Eclipse Ti2E model. The lasers are LaserQuantum solid state gem 532 (1W) and Coherent OBIS 488 nm LS (20 mW). TIRF objective is Nikon Apo TIRF 60X oil immersion objective, NA 1.49. The cameras are an ORCA-Flash4.0 V3 digital CMOS camera from Hamamatsu. Chemicals are from Millipore-Sigma if not specified. More detailed biological preparations are described in ref 38. The details of biomolecule preparation are in Supporting Information.

Single Molecule Data Analysis. For doubly labeled experiments, the acceptor fluorescence intensity is adjusted by subtracting the donor intensity multiplied by the "β" factor. For quadruple-labeled ribosomes, the intensities in the four channels A488, A594, Cy3, and Cy5 are corrected as follows:

$$I_{A488} = I_{A488} - I_{Cy3} \times 4\%$$

$$I_{A594} = I_{A594} - I_{A488} \times 12\% - I_{Cy3} \times 20\%$$

I_{Cy3}: no change

$$I_{Cy5} = I_{Cy5} - I_{Cy3} \times 7\%$$

After these corrections, the FRET efficiencies are calculated according to eq 1 in the main text.

The data analysis follows the approach previously described.[19] Single-molecule traces are first scanned to identify bleaching points, and only fragments before bleaching are analyzed. Selection of single molecule traces is based on the following criteria: 1. The sum of the donor and acceptor intensity must range between 50 to 400; and 2. The Pearson's correlation coefficient between the donor and acceptor traces must be less than −0.6, or between −0.2 to +0.2, providing the ratio between standard variation to the signal average value is less than 20%. The final traces selected are subject to human inspection to exclude any anomalous traces from being selected. Ribosomes carrying both FRET pairs are initially selected on the first 50 data points, with all 100 data points retained in the selected traces. These traces are then selected again based on the second set of 50 data points. Traces that pass both selection criteria are used to generate FRET efficiency histograms for each section. The first half of the data is used to construct a histogram for the Cy3−Cy5 FRET pair, while the second half is utilized to generate the histogram for the Alex 488−594 FRET pair.

ASSOCIATED CONTENT

Supporting Information

The Supporting Information is available free of charge at https://pubs.acs.org/doi/10.1021/cbmi.4c00010.

Biomaterial preparation and two supplemental figures (PDF)

AUTHOR INFORMATION

Corresponding Author

Yuhong Wang − *Department of Biology and Biochemistry, University of Houston, Houston, Texas 77204, United States;* orcid.org/0000-0002-1823-0272; Email: ywang60@uh.edu

Author

Ran Lin − *Department of Biology and Biochemistry, University of Houston, Houston, Texas 77204, United States;* Present Address: Molecular Biosciences Department, The University of Texas at Austin, Austin, Texas 78712, United States

Complete contact information is available at: https://pubs.acs.org/10.1021/cbmi.4c00010

Notes

The authors declare no competing financial interest.

ACKNOWLEDGMENTS

This work is supported by NIGMS grant: R01GM111452, NSF: 2130427, and the Welch Foundation: E-1721 to Y. Wang. We thank the generous large equipment fund from the University of Houston.

REFERENCES

(1) Mohapatra, S.; Lin, C. T.; Feng, X. A.; Basu, A.; Ha, T. Single-Molecule Analysis and Engineering of DNA Motors. *Chem. Rev.* **2020**, *120*, 36−78.

(2) Lerner, E.; Cordes, T.; Ingargiola, A.; Alhadid, Y.; Chung, S.; Michalet, X.; Weiss, S. Toward dynamic structural biology: Two decades of single-molecule Forster resonance energy transfer. *Science* **2018**, *359* (6373), eaan1133.

(3) Ha, T.; Enderle, T.; Chemla, S.; Selvin, R.; Weiss, S. Single Molecule Dynamics Studied by Polarization Modulation. *Phys. Rev. Lett.* **1996**, *77*, 3979−3982.

(4) Blanchard, S. C.; Kim, H. D.; Gonzalez, R. L., Jr.; Puglisi, J. D.; Chu, S. tRNA dynamics on the ribosome during translation. *Proc. Natl. Acad. Sci. U. S. A.* **2004**, *101*, 12893−12898.

(5) Blanchard, S. C.; Gonzalez, R. L.; Kim, H. D.; Chu, S.; Puglisi, J. D. tRNA selection and kinetic proofreading in translation. *Nat. Struct Mol. Biol.* **2004**, *11*, 1008−1014.

(6) Noller, H. F.; Lancaster, L.; Zhou, J.; Mohan, S. The ribosome moves: RNA mechanics and translocation. *Nat. Struct Mol. Biol.* **2017**, *24*, 1021−1027.

(7) Horan, L. H.; Noller, H. F. Intersubunit movement is required for ribosomal translocation. *Proc. Natl. Acad. Sci. U. S. A.* **2007**, *104*, 4881−4885.

(8) Ermolenko, D. N.; Noller, H. F. mRNA translocation occurs during the second step of ribosomal intersubunit rotation. *Nat. Struct Mol. Biol.* **2011**, *18*, 457−462.

(9) Ermolenko, D. N.; Majumdar, Z. K.; Hickerson, R. P.; Spiegel, P. C.; Clegg, R. M.; Noller, H. F. Observation of intersubunit movement of the ribosome in solution using FRET. *J. Mol. Biol.* **2007**, *370*, 530−540.

(10) Schuwirth, B. S.; Borovinskaya, M. A.; Hau, C. W.; Zhang, W.; Vila-Sanjurjo, A.; Holton, J. M.; Cate, J. H. Structures of the bacterial ribosome at 3.5 A resolution. *Science* **2005**, *310*, 827−834.
(11) Frank, J.; Agrawal, R. K. A ratchet-like inter-subunit reorganization of the ribosome during translocation. *Nature* **2000**, *406*, 318−322.
(12) Schmeing, T. M.; Ramakrishnan, V. What recent ribosome structures have revealed about the mechanism of translation. *Nature* **2009**, *461*, 1234−1242.
(13) Gloge, F.; Becker, A. H.; Kramer, G.; Bukau, B. Co-translational mechanisms of protein maturation. *Curr. Opin Struct Biol.* **2014**, *24*, 24−33.
(14) Rexroad, G.; Donohue, J. P.; Lancaster, L.; Noller, H. F. The role of GTP hydrolysis by EF-G in ribosomal translocation. *Proc. Natl. Acad. Sci. U. S. A.* **2022**, *119*, No. e2212502119.
(15) Wasserman, M. R.; Alejo, J. L.; Altman, R. B.; Blanchard, S. C. Multiperspective smFRET reveals rate-determining late intermediates of ribosomal translocation. *Nat. Struct Mol. Biol.* **2016**, *23*, 333−341.
(16) Cornish, P. V.; Ermolenko, D. N.; Noller, H. F.; Ha, T. Spontaneous intersubunit rotation in single ribosomes. *Mol. Cell* **2008**, *30*, 578−588.
(17) Chen, C.; Stevens, B.; Kaur, J.; Cabral, D.; Liu, H.; Wang, Y.; Zhang, H.; Rosenblum, G.; Smilansky, Z.; Goldman, Y. E.; Cooperman, B. S. Single-molecule fluorescence measurements of ribosomal translocation dynamics. *Mol. Cell* **2011**, *42*, 367−377.
(18) Fei, J.; Kosuri, P.; MacDougall, D. D.; Gonzalez, R. L., Jr. Coupling of ribosomal L1 stalk and tRNA dynamics during translation elongation. *Mol. Cell* **2008**, *30*, 348−359.
(19) Altuntop, M. E.; Ly, C. T.; Wang, Y. Single-molecule study of ribosome hierarchic dynamics at the peptidyl transferase center. *Biophysical journal* **2010**, *99*, 3002−3009.
(20) Prabhakar, A.; Puglisi, E. V.; Puglisi, J. D. Single-Molecule Fluorescence Applied to Translation. *Cold Spring Harb Perspect Biol.* **2019**, *11*, a032714.
(21) Feng, X. A.; Poyton, M. F.; Ha, T. Multicolor single-molecule FRET for DNA and RNA processes. *Curr. Opin Struct Biol.* **2021**, *70*, 26−33.
(22) Lee, J.; Lee, S.; Ragunathan, K.; Joo, C.; Ha, T.; Hohng, S. Single-molecule four-color FRET. *Angew. Chem.* **2010**, *49*, 9922−9925.
(23) McCann, J. J.; Choi, U. B.; Zheng, L.; Weninger, K.; Bowen, M. E. Optimizing methods to recover absolute FRET efficiency from immobilized single molecules. *Biophysical journal* **2010**, *99*, 961−970.
(24) Petrychenko, V.; Peng, B.-Z.; de A. P. Schwarzer, A. C.; Peske, F.; Rodnina, M. V.; Fischer, N. Structural mechanism of GTPase-powered ribosome-tRNA movement. *Nat. Commun.* **2021**, *12*, 5933.
(25) Carbone, C. E.; Loveland, A. B.; Gamper, H. B., Jr.; Hou, Y. M.; Demo, G.; Korostelev, A. A. Time-resolved cryo-EM visualizes ribosomal translocation with EF-G and GTP. *Nat. Commun.* **2021**, *12*, 7236.
(26) Gao, Y. G.; Selmer, M.; Dunham, C. M.; Weixlbaumer, A.; Kelley, A. C.; Ramakrishnan, V. The structure of the ribosome with elongation factor G trapped in the posttranslocational state. *Science* **2009**, *326*, 694−699.
(27) Stark, H.; Rodnina, M. V.; Wieden, H. J.; van Heel, M.; Wintermeyer, W. Large-scale movement of elongation factor G and extensive conformational change of the ribosome during translocation. *Cell* **2000**, *100*, 301−309.
(28) Murphy, M. C.; Rasnik, I.; Cheng, W.; Lohman, T. M.; Ha, T. Probing single-stranded DNA conformational flexibility using fluorescence spectroscopy. *Biophysical journal* **2004**, *86*, 2530−2537.
(29) Korostelev, A.; Asahara, H.; Lancaster, L.; Laurberg, M.; Hirschi, A.; Zhu, J.; Trakhanov, S.; Scott, W. G.; Noller, H. F. Crystal structure of a translation termination complex formed with release factor RF2. *Proc. Natl. Acad. Sci. U. S. A.* **2008**, *105*, 19684−19689.
(30) Iqbal, A.; Arslan, S.; Okumus, B.; Wilson, T. J.; Giraud, G.; Norman, D. G.; Ha, T.; Lilley, D. M. Orientation dependence in fluorescent energy transfer between Cy3 and Cy5 terminally attached to double-stranded nucleic acids. *Proc. Natl. Acad. Sci. U. S. A.* **2008**, *105*, 11176−11181.
(31) Fischer, N.; Konevega, A. L.; Wintermeyer, W.; Rodnina, M. V.; Stark, H. Ribosome dynamics and tRNA movement by time-resolved electron cryomicroscopy. *Nature* **2010**, *466*, 329−333.
(32) Zhou, J.; Lancaster, L.; Donohue, J. P.; Noller, H. F. How the ribosome hands the A-site tRNA to the P site during EF-G-catalyzed translocation. *Science* **2014**, *345*, 1188−1191.
(33) Ratje, A. H.; Loerke, J.; Mikolajka, A.; Brunner, M.; Hildebrand, P. W.; Starosta, A. L.; Donhofer, A.; Connell, S. R.; Fucini, P.; Mielke, T.; Whitford, P. C.; Onuchic, J. N.; Yu, Y.; Sanbonmatsu, K. Y.; Hartmann, R. K.; Penczek, P. A.; Wilson, D. N.; Spahn, C. M. Head swivel on the ribosome facilitates translocation by means of intra-subunit tRNA hybrid sites. *Nature* **2010**, *468*, 713−716.
(34) Holtkamp, W.; Cunha, C. E.; Peske, F.; Konevega, A. L.; Wintermeyer, W.; Rodnina, M. V. GTP hydrolysis by EF-G synchronizes tRNA movement on small and large ribosomal subunits. *EMBO J.* **2014**, *33*, 1073−1085.
(35) Wilden, B.; Savelsbergh, A.; Rodnina, M. V.; Wintermeyer, W. Role and timing of GTP binding and hydrolysis during EF-G-dependent tRNA translocation on the ribosome. *Proc. Natl. Acad. Sci. U. S. A.* **2006**, *103*, 13670−13675.
(36) Huang, T.; Choi, J.; Prabhakar, A.; Puglisi, J. D.; Petrov, A. Partial spontaneous intersubunit rotations in pretranslocation ribosomes. *Proc. Natl. Acad. Sci. U. S. A.* **2023**, *120*, No. e2114979120.
(37) Chen, J.; Petrov, A.; Tsai, A.; O'Leary, S. E.; Puglisi, J. D. Coordinated conformational and compositional dynamics drive ribosome translocation. *Nat. Struct Mol. Biol.* **2013**, *20*, 718−727.
(38) Johnson, J. L.; Steele, J. H.; Lin, R.; Stepanov, V. G.; Gavriliuc, M. N.; Wang, Y. Multi-Channel smFRET study reveals a Compact conformation of EF-G on the Ribosome. *BioRxiv*, January 28, 2024. .

https://doi.org/10.1021/cbmi.4c00010
Chem. Biomed. Imaging 2024, 2, 501−509